Available online at www.sciencedirect.com
ScienceDirect
Journal of Sound and Vibration 320 (2009) 163–183
JOURNAL OF SOUND AND VIBRATION
www.elsevier.com/locate/jsvi

Bifurcation analysis of a two-degree-of-freedom aeroelastic system with hysteresis structural nonlinearity by a perturbation-incremental method

K.W. Chung[a,*], Y.B. He[a], B.H.K. Lee[b]

[a]Department of Mathematics, City University of Hong Kong, Tat Chee Avenue, Kowloon, Hong Kong
[b]Aerodynamics Laboratory, National Research Council, Institute for Aerospace Research, Ottawa, Ontario, Canada K1A 0R6

Received 10 April 2008; received in revised form 8 July 2008; accepted 12 July 2008
Handling Editor: L.G. Tham
Available online 3 September 2008

Abstract

A perturbation-incremental (PI) method is presented for the computation, continuation and bifurcation analysis of limit cycle oscillations (LCO) of a two-degree-of-freedom aeroelastic system containing a hysteresis structural nonlinearity. Both stable and unstable LCOs can be calculated to any desired degree of accuracy and their stabilities are determined by the theory of Poincaré map. Thus, the present method is capable of detecting complex aeroelastic responses such as periodic motion with harmonics, period-doubling, saddle-node bifurcation, Neimark–Sacker bifurcation and the coexistence of limit cycles. The dynamic response is quite different from that of an aeroelastic system with freeplay structural nonlinearity. New phenomena are observed in that the emanating branches from period-doubling bifurcations are not smooth and the bifurcation of a LCO may lead to the simultaneous coexistence of all period-2^n LCOs.

1. Introduction

The study of the dynamic behavior of aircraft structures is crucial in flutter analysis since it provides useful information in the design of aircraft wings and control surfaces. Concentrated structural nonlinearities can have significant effects on the aeroelastic responses of aerosurfaces even for small vibrational amplitudes. There are three types of nonlinearities in concentrated nonlinear structures, namely cubic, freeplay and hysteresis stiffnesses. The former two types have been extensively studied by many investigators. Aeroelastic systems with cubic stiffness have been successfully analyzed by using the describing function [1], harmonic balance method [2], the center manifold and the principle of normal form [3]. The describing function method [4], the rational polynomial approximation [5] and the point transformation (PT) method [6] were applied to analyze the aeroelastic system with a freeplay model. Trickey et al. [7] investigated both local and global stability of an airfoil with a freeplay nonlinearity based on both experimental and numerical studies. A survey of different types of nonlinearity and their effect on aeroelastic behavior can be found in Refs. [8,9].

*Corresponding author. Tel.: +852 27888671; fax: +852 27888561.
E-mail address: makchung@cityu.edu.hk (K.W. Chung).

0022-460X/$ - see front matter
doi:10.1016/j.jsv.2008.07.019

Compared to the study of cubic and freeplay nonlinearities, much less literature has been found on the study of hysteresis nonlinearity. A comprehensive survey can be found in Ref. [10]. The main drawback of using harmonic balance methods to investigate freeplay and hysteresis nonlinearities is that the second derivative of an approximate solution obtained by such methods is continuous while that of the exact solution is discontinuous at the switching points where changes in linear subdomains occur. Such inconsistency between the exact and the approximate solutions may lead to serious error in the prediction and analysis. To overcome this drawback, Liu et al. [6,10] employed the PT method which can track the system behavior to the exact point where the change in linear subdomains occurs. However, the PT method is not capable of finding unstable periodic solutions and thus is not suitable for performing parametric continuation.

On the other hand, nonlinearities of hysteresis type are common in many different areas of science and technology, including physics, biology, mechanics and electronics. The phenomenon of hysteresis has been recently attracting the attention of many investigators. Practical models of hysteresis can be found in Refs. [11,12]. The folding mechanism of many chaotic circuits is based on hysteresis nonlinearity [13].

In view of the above situation, we consider developing a general method for the study of limit cycle oscillation (LCO) of aeroelastic system with hysteresis nonlinearity, which may also be extended to investigate other models of hysteresis. Chung et al. [14] applied a perturbation-incremental (PI) method to study LCOs and bifurcation of an aeroelastic model with freeplay nonlinearity. The PI method is a semi-analytical and numerical process which incorporates salient features from both the perturbation method and the incremental approach. Both stable and unstable LCOs can be calculated accurately. The continuation curves thus give a full picture of the global bifurcation.

In this paper, we extend the PI method to the continuation and bifurcation analysis of an aeroelastic model with hysteresis nonlinearity. In fact, the method can also be applied to any piecewise-linear system with hysteresis nonlinearity. The paper is organized as follows. A brief description of an aeroelastic model with hysteresis nonlinearity is given in Section 2. In Section 3, we discuss the solution type of LCO in each linear region. The PI method is described in Section 4. Bifurcation analysis is discussed in Section 5, followed by conclusions in Section 6.

2. The mathematical model

Fig. 1 shows a sketch of a two-degree-of-freedom (2-dof) airfoil motion in plunge and pitch. The plunge deflection is denoted by h, positive in the downward direction, and α is the pitch angle about the elastic axis, positive nose up.

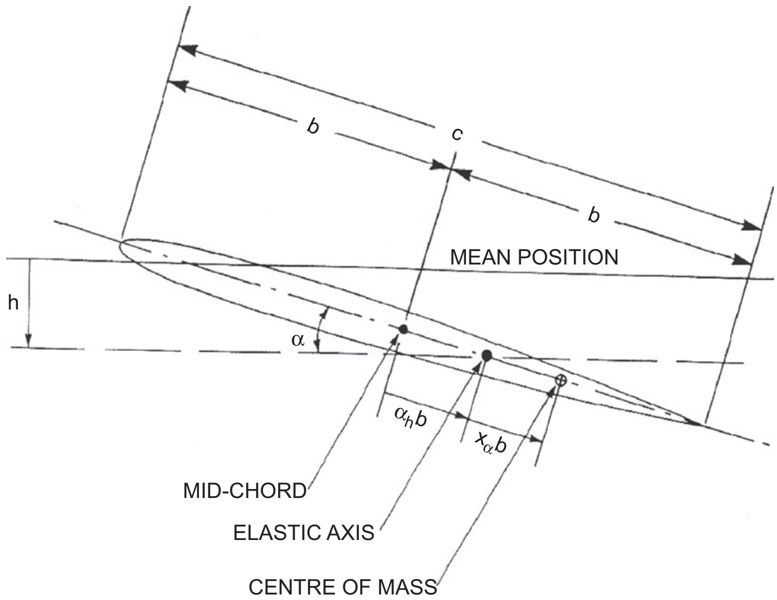

Fig. 1. Schematic of airfoil with 2 dof motion.

The elastic axis is located at a distance $a_h b$ from the mid-chord, while the mass center is located at a distance $x_a b$ from the elastic axis, where b is the airfoil semi-chord. Both distances are positive when measured towards the trailing edge of the airfoil. The aeroelastic equations of motion for linear springs have been derived by Fung [15]. For nonlinear restoring forces, the coupled bending–torsion equations for the airfoil can be written as follows:

$$m\ddot{h} + S\ddot{\alpha} + C_h\dot{h} + \bar{G}(h) = p(t), \tag{1}$$

$$S\ddot{h} + I_\alpha\ddot{\alpha} + C_\alpha\dot{\alpha} + \bar{M}(\alpha) = r(t), \tag{2}$$

where the symbols m, S, C_h, I_α and C_α are the airfoil mass, airfoil static moment about the elastic axis, damping coefficient in plunge, wing mass moment of inertia about elastic axis, and torsion damping coefficient, respectively. $\bar{G}(h)$ and $\bar{M}(\alpha)$ are the nonlinear plunge and pitch stiffness terms, and $p(t)$ and $r(t)$ are the forces and moments acting on the airfoil, respectively. By a suitable transformation as described in Refs. [6,16,17], the airfoil motion without any external forces can be rewritten into a system of eight first-order ordinary differential equations:

$$\begin{aligned}
x_1' &= x_2,\\
x_2' &= \sum_{i=1}^{8} a_{2i}x_i + j\left[d_0\left(\frac{\bar{\omega}}{U^*}\right)^2 G(x_3) - c_0\left(\frac{1}{U^*}\right)^2 M(x_1)\right],\\
x_3' &= x_4,\\
x_4' &= \sum_{i=1}^{8} a_{4i}x_i + j\left[c_1\left(\frac{1}{U^*}\right)^2 M(x_1) - d_1\left(\frac{\bar{\omega}}{U^*}\right)^2 G(x_3)\right],\\
x_5' &= x_1 - \varepsilon_1 x_5,\\
x_6' &= x_1 - \varepsilon_2 x_6,\\
x_7' &= x_3 - \varepsilon_1 x_7,\\
x_8' &= x_3 - \varepsilon_2 x_8,
\end{aligned} \tag{3}$$

where the $'$ denotes differentiation with respect to the non-dimensional time τ defined by $\tau = Ut/b$ with U being the free-stream velocity. The coefficients $j, a_{21}, \ldots, a_{28}, a_{41}, \ldots, a_{48}, c_0, c_1, d_0, d_1, \varepsilon_1$ and ε_2 are related to the system parameters and their expressions are given in Appendix A. The structural nonlinearities are represented by the nonlinear functions $G(x_3)$ and $M(x_1)$. In this paper, we investigate system (3) for a hysteresis damper in pitch and a linear spring in plunge, i.e. $G(x_3) = x_3$. The hysteretic damper consists of a linear elastic spring and a coulomb damper with amplitude constraint in two directions. For detailed description of such damper, see p. 15 of Ref. [11] or p. 97 of Ref. [18]. The hysteresis stiffness $M(x_1)$ is described by the line segments I–V as shown in Fig. 2.

Notice that I, III and V are bidirectional while II and IV are unidirectional. The boundary of the hysteresis is composed of two freeplays following specified directions. If the traveling path is along the upper branch of the hysteresis, i.e. I → II → III with x_1 increasing, then $M(x_1)$ is given by

$$M(x_1) = \begin{cases} x_1 + M_0 - \alpha_f, & x_1 < \alpha_f \uparrow,\\ M_f x_1 + M_0 - \alpha_f M_f, & \alpha_f \leqslant x_1 \leqslant \alpha_f + \delta \uparrow,\\ x_1 + M_0 - \alpha_f - \delta(1 - M_f), & x_1 > \alpha_f + \delta \uparrow, \end{cases} \tag{4a}$$

where $\uparrow$ represents the motion in the increasing x_1 direction. M_0, M_f, α_f and δ are constants. On the other hand, if the traveling path is along the lower branch, i.e. III → IV → I with x_1 decreasing, then

$$M(x_1) = \begin{cases} x_1 - M_0 + \alpha_f + \delta(1 - M_f), & x_1 < -\alpha_f - \delta \downarrow,\\ M_f x_1 - M_0 + \alpha_f M_f, & -\alpha_f - \delta \leqslant x_1 \leqslant -\alpha_f \downarrow,\\ x_1 - M_0 + \alpha_f, & x_1 > -\alpha_f \downarrow, \end{cases} \tag{4b}$$

where $\downarrow$ represents the motion in the decreasing x_1 direction. Without loss of generality, let $\alpha_f = M_0 - (\delta/2)(1 - M_f)$. Then, in Eqs. (4a) and (4b), we have $x_1 + M_0 - \alpha_f = x_1 - M_0 + \alpha_f + \delta(1 - M_f)$ and

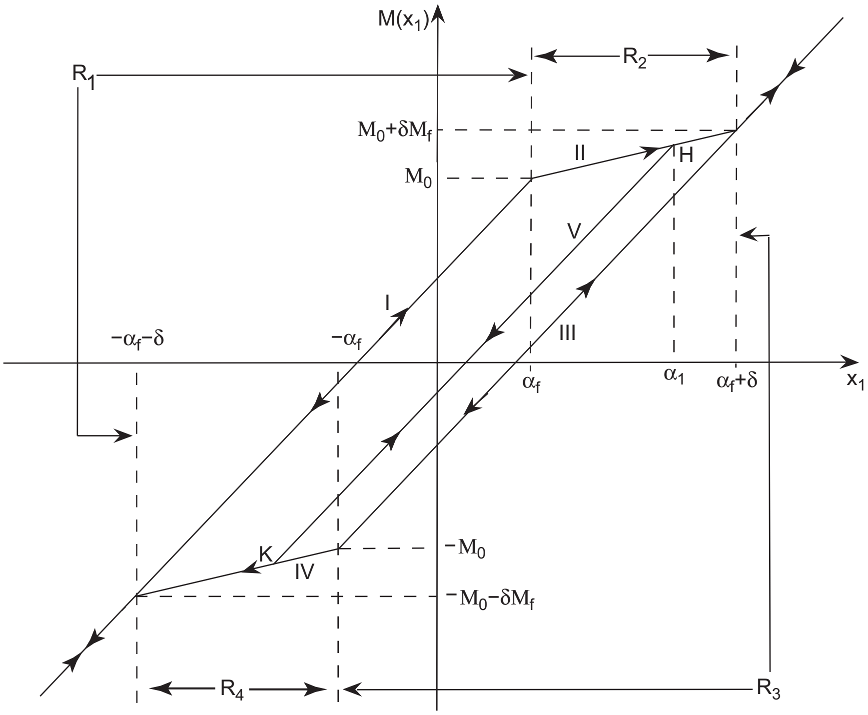

Fig. 2. General sketch of a hysteresis stiffness.

$x_1 + M_0 - \alpha_f - \delta(1 - M_f) = x_1 - M_0 + \alpha_f$. In a concise form, Eqs. (4a) and (4b) can be rewritten as

$$M(x_1) = \begin{cases} x_1 + \frac{M_f - 1}{2}(|x_1 - \alpha_f| - |x_1 - \alpha_f - \delta|), & x_1 \uparrow, \quad (4a') \\ x_1 + \frac{M_f - 1}{2}(|x_1 + \alpha_f + \delta| - |x_1 + \alpha_f|), & x_1 \downarrow. \quad (4b') \end{cases}$$

Furthermore, when the traveling path is along II (IV, resp.), $x_2 = x_1'$ may become zero. If x_1 changes direction at, say, point H (K, resp.), x_1' becomes negative (positive, resp.). Then, $M(x_1)$ switches to line segment V which is parallel to both I and III. Let α_1 be the abscissa of H which is the intersection point of line segments II and V. The equation of line segment V is given by

$$M(x_1) = x_1 + M_0 - \alpha_1 + M_f(\alpha_1 - \alpha_f), \quad \alpha_1 - 2\alpha_f - \delta \leqslant x_1 \leqslant \alpha_1 \uparrow\downarrow, \tag{4c}$$

where $\alpha_f \leqslant \alpha_1 \leqslant \alpha_f + \delta$. The hysteresis model described in Eqs. (4a)–(4c) is more general than that defined in Ref. [10], since $M_f \neq 0$ and $M(x_1)$ is also defined inside the hysteresis loop.

Fig. 2 shows the four main regions R_j ($j = 1, 2, 3, 4$) which correspond to the following linear subsystems and associate with line segments $i = \mathrm{I, II, III, IV}$, respectively,

$$\text{(I)} \quad X' = AX + F_1, \quad x_1 < \alpha_f \uparrow\downarrow, \tag{5a}$$

$$\text{(II)} \quad X' = BX + F_2, \quad \alpha_f \leqslant x_1 \leqslant \alpha_f + \delta \uparrow, \tag{5b}$$

$$\text{(III)} \quad X' = AX - F_1, \quad x_1 > -\alpha_f \uparrow\downarrow, \tag{5c}$$

$$\text{(IV)} \quad X' = BX - F_2, \quad -\alpha_f - \delta \leqslant x_1 \leqslant -\alpha_f \downarrow. \tag{5d}$$

The elements of A, B and F_i ($i = 1, 2$) are determined by the system parameters of the coupled aeroelastic equations, and they are given by

$$A = \begin{pmatrix} A_1 & A_2 \\ A_3 & A_4 \end{pmatrix}, \quad B = \begin{pmatrix} B_1 & A_2 \\ A_3 & A_4 \end{pmatrix} \tag{6}$$

and $F_1 = (M_0 - \alpha_f)F$, $F_2 = (M_0 - \alpha_f M_f)F$, where A_i $(i = 1, 2, 3, 4)$, B_1 and the vector F are defined in Appendix B with $\beta = 1$.

Unlike the freeplay model, the number of linear regions created in the phase space $X \in \mathbb{R}^8$ due to a LCO may not be fixed. It may happen that the trajectory of a LCO changes direction when moving along line segment II or IV. Then, a new linear region R_5 is created corresponding to the linear subsystem

$$\text{(V)} \quad X' = AX + F_3, \quad \alpha_1 - 2\alpha_f - \delta < x_1 < \alpha_1 \uparrow\downarrow, \tag{5e}$$

where $F_3 = [M_0 - \alpha_1 + M_f(\alpha_1 - \alpha_f)]F$ and α_1 is the abscissa of the intersection point of line segments II and V such that $\alpha_f \leqslant \alpha_1 \leqslant \alpha_f + \delta$.

3. LCO and solution type

Consider the hysteresis model shown in Fig. 2. Let the $Z - Y$ plane represent the eight-dimensional phase space, where $Z = \{x_1\}$ and $Y = \{x_2, \ldots, x_8\}$. We first of all consider a LCO traveling only in the four main regions R_j $(j = 1, 2, 3, 4)$. Let Z_1, Z_2, Z_3 and Z_4 denote the switching subspaces $Z = -\alpha_f - \delta$, $Z = \alpha_f$, $Z = \alpha_f + \delta$ and $Z = -\alpha_f$, respectively, where the linear systems change (see Fig. 3(a)). The system response can be predicted by following a general phase path. Assuming that a motion initially starts at a point X_1 in one of the switching subspaces (say Z_1) as shown in Fig. 3(a), the trajectory travels in R_i $(i = 1, 2, 3)$, hits Z_{i+1} at X_{i+1} and eventually hits Z_1 again at X_5. The points X_i $(i = 1, \ldots, 5)$ are called switching points as they are located in the switching subspaces. We note that the points X_1 and X_5 define a Poincarè map in Z_1. The trajectory becomes a LCO if X_5 coincides with X_1 (see Fig. 3(b)). Since the system of equations in each region is strictly linear, the exact solutions in R_i can be obtained analytically. Therefore, for a given point X_1 in Z_1, X_5 can be determined analytically.

Next, we consider the case when the trajectory of a LCO changes direction at H in Fig. 2 when moving along line segment II. In the phase space shown in Fig. 3(c), the trajectory intersects tangentially a new switching subspace Z_5, given by $Z = \alpha_1$ at X_6. A new region R_5 is created corresponding to the traveling path along line segment V. If the trajectory does not move as far back as to point K which is the intersection of line segments IV and V, it stays in R_5 and hits Z_5 again at X_7. Thus, a change of direction along II or IV creates a new switching subspace and gives arise to a harmonic component in a LCO.

Finally, we consider the analytic expression of trajectory in each linear region starting with R_2 which corresponds to the linear subsystem (5b). Note that $\det(B) = 0$ and $\operatorname{rank}(B) = 7$.

Proposition 1. *If F_2 in Eq.* (5b) *is non-zero, then the system of equations*

$$BX + F_2 = 0 \tag{7}$$

has no solution.

Proof. Let $X = (x_1, \ldots, x_8)^{\mathrm{T}}$. From Appendices A and B for the definition of matrices B, F_2 and Eq. (7) above, we have $x_2 = x_4 = 0$, $x_5 = x_1/\varepsilon_1$, $x_6 = x_1/\varepsilon_2$, $x_7 = x_3/\varepsilon_1$, $x_8 = x_3/\varepsilon_2$ and

$$\begin{aligned} &\begin{pmatrix} b_{21} + a_{25}/\varepsilon_1 + a_{26}/\varepsilon_2 & b_{23} + a_{27}/\varepsilon_1 + a_{28}/\varepsilon_2 \\ b_{41} + a_{45}/\varepsilon_1 + a_{46}/\varepsilon_2 & b_{43} + a_{47}/\varepsilon_1 + a_{48}/\varepsilon_2 \end{pmatrix} \begin{pmatrix} x_1 \\ x_3 \end{pmatrix} \\ &\quad = (M_f \alpha_f - M_0) j \left(\frac{1}{U^*} \right)^2 \begin{pmatrix} -c_0 \\ c_1 \end{pmatrix}, \end{aligned} \tag{8}$$

where b_{21}, b_{23}, b_{41} and b_{43} are the corresponding elements of the matrix $B = (b_{ik})$. The determinant of the 2×2 matrix in (8) is zero. Furthermore,

$$\begin{vmatrix} b_{21} + a_{25}/\varepsilon_1 + a_{26}/\varepsilon_2 & -c_0 \\ b_{41} + a_{45}/\varepsilon_1 + a_{46}/\varepsilon_2 & c_1 \end{vmatrix} = (c_1 d_0 - c_0 d_1)(c_5 + c_6/\varepsilon_1 + c_7/\varepsilon_2), \tag{9}$$

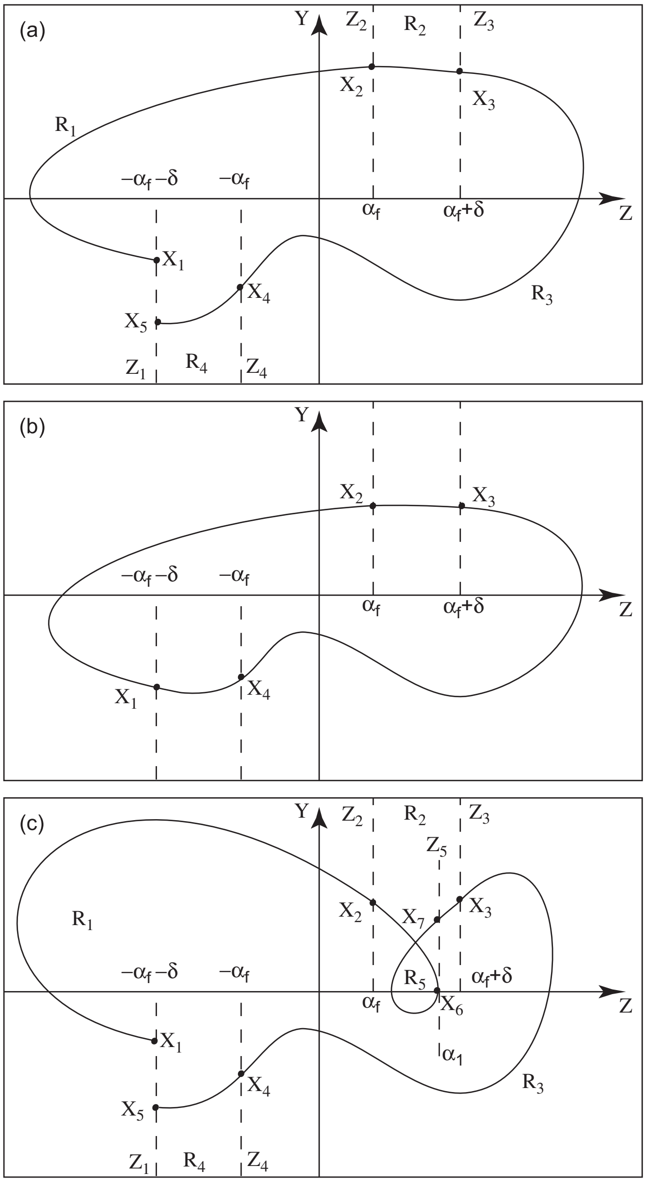

Fig. 3. Phase portrait of the aeroelastic system (3) with hysteresis structure: (a) general trajectory; (b) period-one LCO; (c) trajectory where the traveling path branches off from II to V.

where c_i and d_i are defined in Appendix A. Since $c_1d_0 - c_0d_1 = -1/j \neq 0$ and $c_5 + c_6/\varepsilon_1 + c_7/\varepsilon_2 = 2/\mu$, the expression of Eq. (9) is non-zero. Therefore, Eq. (8) and, equivalently, Eq. (7) have no solution. This completes the proof. □

The consequence of Proposition 1 is that a linear combination of eight independent vectors is required to describe a trajectory in R_2 (and R_4). This is different from the freeplay model studied in Ref. [14] in which a trajectory in R_2 travels in a seven-dimensional submanifold. In the following, we replace the non-dimensional time τ by t.

Proposition 2. *Let* $\mathbf{v}_i$ $(i = 1, \ldots, 7)$ *and* $\mathbf{v}_8$ *be the eigenvectors of B corresponding to the non-zero eigenvalues* λ_i *and the zero eigenvalue* λ_8 $(= 0)$, *respectively. Then, a solution of Eq.* (5b) *is expressed as*

$$\mathbf{r}(t) = \sum_{i=1}^{7} p_i \mathbf{v}_i + t p_8 \mathbf{v}_8 + \sum_{i=1}^{8} k_i\, \mathbf{e}^{\lambda_i t} \mathbf{v}_i, \tag{10}$$

where k_i ($i = 1, \ldots, 8$) are arbitrary constants depending on initial condition and

$$(p_1 \ \ldots \ p_8)^{\mathrm{T}} = (-\lambda_1 \mathbf{v}_1 \ \ldots \ -\lambda_7 \mathbf{v}_7 \ \mathbf{v}_8)^{-1} F_2. \tag{11}$$

Proof. Since $\operatorname{rank}(B) = 7$, a solution of Eq. (5b) can be expressed in the form

$$\mathbf{r}(t) = \mathbf{p} + t p_8 \mathbf{v}_8 + \sum_{i=1}^{8} k_i \, \mathrm{e}^{\lambda_i t} \mathbf{v}_i, \tag{12}$$

where $k_i \in \mathbb{R}$, $p_8 \in \mathbb{R}$ and $\mathbf{p}$ is a constant vector in the subspace spanned by $\mathbf{v}_i$ ($i = 1, \ldots, 7$). Thus, we let $\mathbf{p} = \sum_{i=1}^{7} p_i \mathbf{v}_i$. Differentiating Eq. (12) with respect to t and substituting it into Eq. (5b), we obtain, after simplification,

$$p_8 \mathbf{v}_8 = \sum_{i=1}^{7} p_i \lambda_i \mathbf{v}_i + F_2,$$

which implies Eq. (11). This completes the proof. $\square$

The analytic expression of trajectory in region R_4 is the same as Eq. (10) with F_2 in Eq. (11) replaced by $-F_2$.

Since $\det(A) \neq 0$ in the regions R_1, R_3 and R_5, a trajectory $\mathbf{r}(t)$ in these regions is simply expressed analytically as

$$\mathbf{r}(t) = \mathbf{u} + \sum_{i=1}^{8} k_i \, \mathrm{e}^{\lambda_i t} \mathbf{v}_i, \tag{13}$$

where $k_i \in \mathbb{R}$, λ_i and $\mathbf{v}_i$ are the eigenvalues and the corresponding eigenvectors of A, respectively. The constant vector $\mathbf{u}$ is equal to $-A^{-1}F_1$, $A^{-1}F_1$ and $-A^{-1}F_3$ if $\mathbf{r}(t)$ is in regions R_1, R_3 and R_5, respectively.

4. The perturbation-incremental (PI) method

The main idea of the PI method is to convert a LCO to an equilibrium point of a Poincaré map in a switching subspace and consider a system of variational equations of the map for parametric continuation. Same as in Refs. [6,14], the non-dimensional velocity U^* is mainly used as the bifurcation parameter. The procedure of the PI method is divided into two steps. The first step is to obtain an initial solution for the continuation of the bifurcation parameter in the second step. A matrix dimension reduction technique is employed to speed up the computations involved in the second step.

4.1. Perturbation step

For a smooth dynamical system, small LCO can be obtained through Hopf bifurcation. However, Hopf bifurcation theorems cannot be applied to a piecewise-linear system due to its low differentiability. Nevertheless, a piecewise-linear system can undergo bifurcations which have similarities (but also discrepancies) with the Hopf bifurcation [19]. System (3) with hysteresis nonlinearity defined in Eqs. (4a)–(4c) is a symmetric piecewise-linear system. A system of the form $X' = F(X)$ with $X \in \mathbb{R}^n$ is symmetric if it satisfies the condition $F(-X) = -F(X)$. A LCO is symmetric if $X(t + T/2) = -X(t)$ where T is the period. An initial symmetric LCO may be obtained in the following way.

We first consider a symmetric periodic solution traveling only in R_5 which corresponds to line segment V passing through the origin as shown in Fig. 4(a). From Eq. (4c), the abscissa of H is given by

$$\alpha_1 = \alpha_f + \frac{\delta}{2}. \tag{14}$$

The necessary condition for the existence of periodic solution in the linear subspace R_5 is that a pair of eigenvalues of matrix A become pure imaginary (say $\lambda = \pm \mathrm{i}\omega$, $\omega > 0$) at a specific value of the bifurcation parameter U^*. Let $\mathbf{u}_1 \pm \mathrm{i}\mathbf{u}_2$ be the corresponding eigenvectors. The calculation of initial periodic solution below is similar to that for the freeplay model in Ref. [14]. A periodic solution spanned by $\mathbf{u}_1$ and $\mathbf{u}_2$ in R_5 can be expressed as

$$\mathbf{r}(t) = (p_1 + \mathrm{i}p_2)(\mathbf{u}_1 + \mathrm{i}\mathbf{u}_2)\mathrm{e}^{\mathrm{i}\omega t} + (p_1 - \mathrm{i}p_2)(\mathbf{u}_1 - \mathrm{i}\mathbf{u}_2)\mathrm{e}^{-\mathrm{i}\omega t} - A^{-1}F_3, \tag{15}$$

where $p_1, p_2 \in \mathbb{R}$ and α_1 in F_3 is given in Eq. (14). Let Z_1 and Z_2 be the switching subspaces $Z = -\alpha_1$ and $Z = \alpha_1$, respectively (see Fig. 4(a)). If the linear subspace spanned by $\mathbf{u}_1$ and $\mathbf{u}_2$ intersects both Z_1 and Z_2, then there exists a unique periodic solution intersecting tangentially these two switching subspaces with maximal amplitude. Let $\mathbf{r}(0)$ and $\mathbf{r}(T/2)$ be the switching points at Z_1 and Z_2, respectively, where T is the period. From Eq. (15) and the fact that the tangent at $\mathbf{r}(0)$ is orthogonal to the Z-axis, we have

$$\begin{cases} p_1 u_{11} - p_2 u_{21} = -\dfrac{\alpha_1}{2}, \\ p_2 u_{11} + p_1 u_{21} = 0, \end{cases}$$

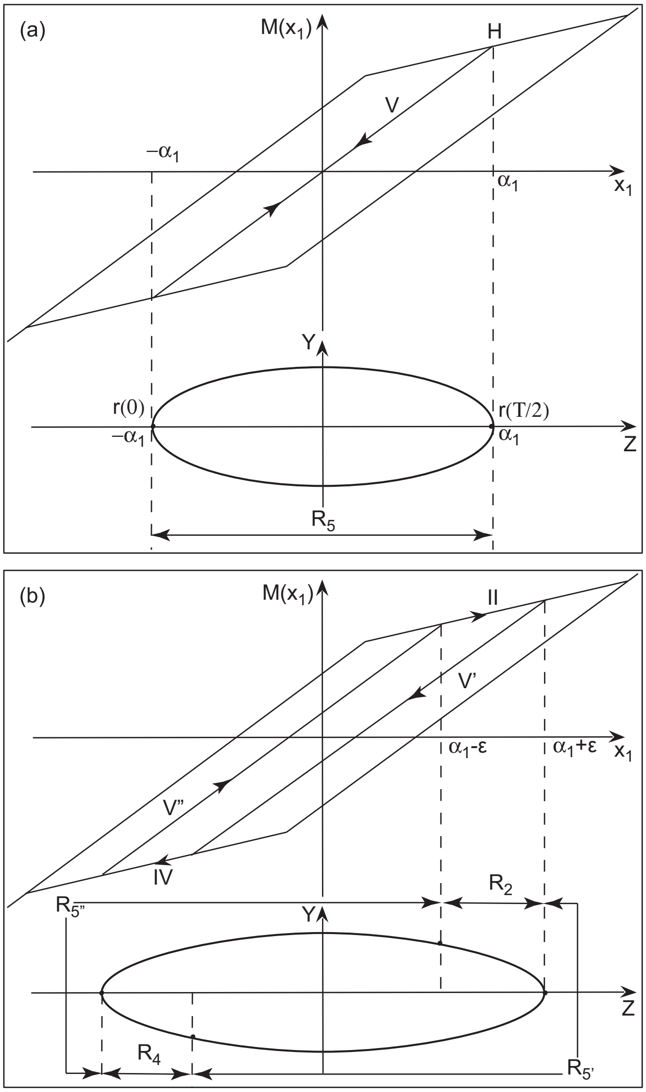

Fig. 4. (a) Periodic solution with maximal amplitude in the linear subspace spanned by $\mathbf{u}_1$ and $\mathbf{u}_2$ and (b) symmetric LCO traveling from regions created by a perturbation from the critical value.

which imply

$$p_1 = \frac{-\alpha_1 u_{11}}{2(u_{11}^2 + u_{21}^2)} \quad \text{and} \quad p_2 = \frac{\alpha_1 u_{21}}{2(u_{11}^2 + u_{21}^2)}, \tag{16}$$

where u_{i1} $(i = 1,2)$ are the first components of $\mathbf{u}_i$. As the bifurcation parameter is varied from the critical value, a symmetric LCO traversing four regions as shown in Fig. 4(b) may suddenly appear. For small ε, the LCO is tangential to both the switching subspaces $Z = -\alpha_1 - \varepsilon$ and $Z = \alpha_1 + \varepsilon$.

4.2. Parameter incremental step—a Newton–Raphson procedure

Contrary to the freeplay nonlinearity, the parameter incremental step for the hysteresis nonlinearity needs to take into account the unidirectional condition of line segments II and IV of $M(x_1)$, and the fact that a trajectory may travel in R_5 which corresponds to line segment V. Assume that a LCO contains n switching points X_i $(i = 1,2,\ldots,n)$ (see Fig. 5). Let $\mathbf{r}_i(t)$ $(i = 1,2,\ldots,n)$ be the segment of LCO between X_i and X_{i+1} with $X_{n+1} = X_1$ traveling in region R_{p_i} $(p_i \in \{1,2,3,4,5\})$. From Eqs. (10), (11) and (13), $\mathbf{r}_i(t)$ may be expressed in the following analytical form:

$$\mathbf{r}_i(t) = \mathbf{u}_{p_i} + \sum_{j=1}^{8} k_{ij}\, \mathrm{e}^{\lambda_{p_i j} t} \mathbf{v}_{p_i j}, \tag{17}$$

where $k_{ij} \in \mathbb{R}$, $\lambda_{p_i j}$ and $\mathbf{v}_{p_i j}$ are the eigenvalues and eigenvectors, respectively, of matrices A if $p_i = 1,3,5$ and B if $p_i = 2,4$, and

$$\mathbf{u}_{p_i} = \begin{cases} -A^{-1}F_1 & \text{if } p_i = 1, \\ CF_2 & \text{if } p_i = 2, \\ A^{-1}F_1 & \text{if } p_i = 3, \\ -CF_2 & \text{if } p_i = 4, \\ -A^{-1}F_3 & \text{if } p_i = 5 \end{cases} \tag{17a}$$

with $C = (\mathbf{v}_{p_i 1}\ \mathbf{v}_{p_i 2}\ \ldots\ \mathbf{v}_{p_i 7}\ t\mathbf{v}_{p_i 8})(-\lambda_{p_i 1}\mathbf{v}_{p_i 1}\ -\lambda_{p_i 2}\mathbf{v}_{p_i 2}\ \ldots\ -\lambda_{p_i 7}\mathbf{v}_{p_i 7}\ \mathbf{v}_{p_i 8})^{-1}$. We note that $\mathbf{u}_{p_i}$ is a function of t only if $p_i = 2,4$. If t in $\mathbf{r}_i(t)$ counts only the time traveled in R_{p_i} with traveling time t_i from X_i to X_{i+1}, we have

$$X_i = \mathbf{r}_i(0) = \mathbf{r}_{i-1}(t_{i-1}), \quad i = 1,2,\ldots,n, \tag{18}$$

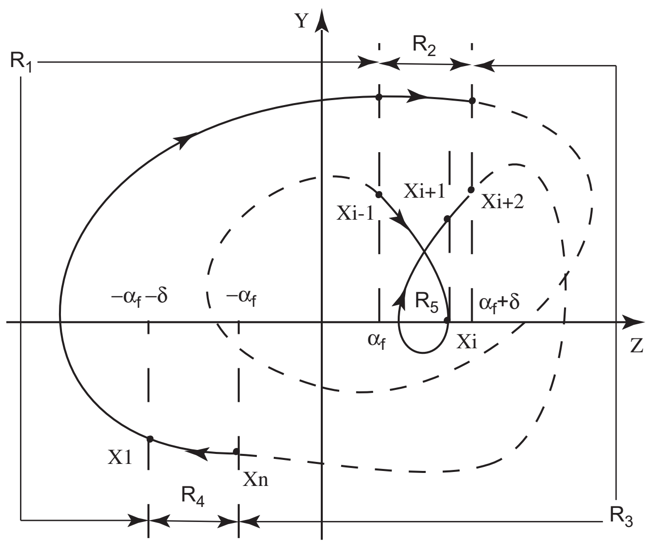

Fig. 5. A general LCO.

with subscript '0' replaced by 'n' (i.e. $\mathbf{r}_0(t_0) = \mathbf{r}_n(t_n)$). This replacement of subscript '0' by 'n' will also be adopted in subsegment formulae derived from Eq. (18). Substituting Eq. (17) into Eq. (18), we obtain

$$X_i = \mathbf{u}_{p_i}|_{t=0} + \sum_{j=1}^{8} k_{ij}\mathbf{v}_{p_ij} = \mathbf{u}_{p_{i-1}}|_{t=t_{i-1}} + \sum_{j=1}^{8} k_{(i-1)j}\mathrm{e}^{\lambda_{p_{i-1}j}t_{i-1}}\mathbf{v}_{p_{i-1}j}, \quad i = 1, 2, \ldots, n. \tag{19}$$

The period of a LCO is given by $T = \sum_{i=1}^{n} t_i$.

In solving Eq. (18) for X_i's, the unknowns in a switching point at the boundary of R_5 are different from those of a switching point at the intersection of two main regions. The first component of a latter switching point is constant while the other seven components are unknowns to be determined in the incremental step. In the general LCO of Fig. 5, let X_i and X_{i+1} be the switching points at the boundary of R_5. Since the trajectory branches off to line segment V at X_i and gets back to line segment II at X_{i+1}, the second component of X_i is zero and both X_i and X_{i+1} have the same first component. Therefore, the first component of these two switching points is an unknown although they have also an average of seven unknowns. To consider the continuation in U^*, a small increment of U^* to $U^* + \Delta U^*$ in Eq. (19) corresponds to small changes of the following quantities:

$$X_i \to X_i + \Delta X_i, \quad k_{ij} \to k_{ij} + \Delta k_{ij}, \quad \mathbf{u}_{p_{i-1}} \to \mathbf{u}_{p_{i-1}} + \Delta\mathbf{u}_{p_{i-1}} \quad \text{and} \quad t_{i-1} \to t_{i-1} + \Delta t_{i-1}.$$

To obtain a neighboring solution, Eq. (19) is expanded in Taylor's series about an initial solution. Linearized incremental equations are derived by ignoring all the nonlinear terms of small increments as below:

$$\begin{aligned} X_i + \Delta X_i &= \mathbf{u}_{p_i}|_{t=0} + \sum_{j=1}^{8} k_{ij}\mathbf{v}_{p_ij} + \sum_{j=1}^{8} \Delta k_{ij}\mathbf{v}_{p_ij} \\ &= \mathbf{u}_{p_{i-1}}|_{t=t_{i-1}} + \sum_{j=1}^{8} k_{(i-1)j}\,\mathrm{e}^{\lambda_{p_{i-1}j}t_{i-1}}\mathbf{v}_{p_{i-1}j} + \Delta\mathbf{u}_{p_{i-1}} \\ &\quad + \sum_{j=1}^{8} \Delta k_{(i-1)j}\,\mathrm{e}^{\lambda_{p_{i-1}j}t_{i-1}}\mathbf{v}_{p_{i-1}j} \\ &\quad + \Delta t_{i-1}\sum_{j=1}^{8} \lambda_{p_{i-1}j}k_{(i-1)j}\,\mathrm{e}^{\lambda_{p_{i-1}j}t_{i-1}}\mathbf{v}_{p_{i-1}j}, \quad i = 1, 2, \ldots, n. \end{aligned} \tag{20}$$

Let q be the eighth component of the column vector

$$(-\lambda_{p_{i-1}1}v_{p_{i-1}1} \quad -\lambda_{p_{i-1}2}v_{p_{i-1}2} \quad \ldots \quad -\lambda_{p_{i-1}7}v_{p_{i-1}7} \;\; v_{p_{i-1}8})^{-1}F_2.$$

It follows from Eq. (17a) that $\Delta\mathbf{u}_{p_{i-1}}$ in Eq. (20) is given by

$$\Delta\mathbf{u}_{p_{i-1}} = \begin{cases} \Delta t_{i-1}qv_{p_{i-1}8}, & \text{if } p_{i-1} = 2, \\ -\Delta t_{i-1}qv_{p_{i-1}8}, & \text{if } p_{i-1} = 4, \\ 0, & \text{otherwise.} \end{cases} \tag{20a}$$

As the bifurcation parameter U^* varies, the number n of switching points of a LCO may become quite large after several bifurcations. To solve Eq. (20) in an efficient way for large n, a matrix dimension reduction technique described in Ref. [14] is used, which is a part of the PI method for non-smooth systems.

In Fig. 3, the switching points of a trajectory in a particular switching subspace define a Poincaré map. The eigenvalues of the first derivative of a Poincaré map evaluated at a fixed point determine the stability of a LCO. The details are given in Section 4 of Ref. [14]. For a general LCO with n switching points, the Jacobian matrix of the Poincaré map is the product of n matrices which follows from the chain rule. For freeplay nonlinearity, the dimension of each matrix is 7×7. However, for the hysteresis nonlinearity, the dimension of a matrix may be different. In Fig. 5, consider the trajectory in region R_5 with boundary switching point X_i and X_{i+1}. We note that X_i has seven unknowns since the second component is zero and X_{i+1} has eight unknowns. Therefore, the dimension of the matrix corresponding to this trajectory segment is 7×8. In Fig. 5, we may assume that X_{i+2} has seven unknowns and the first component is a constant. Then, the dimension of the matrix corresponding to this trajectory segment is 8×7. Therefore, the dimension of the matrix corresponding to the trajectory segment from X_i to X_{i+2} is still 7×7. The overall calculation of the Jacobian matrix for stability is more or less the same as that in Ref. [14].

5. Results and discussions

To compare with the previous results obtained in Ref. [10], the system parameters under consideration are chosen as

$$\mu = 100, \quad a_h = -0.5, \quad x_\alpha = 0.25, \quad \zeta_\xi = \zeta_\alpha = 0, \quad \gamma_\alpha = 0.5 \quad \text{and} \quad \bar{\omega} = 0.2.$$

The pitch angle is hysteretic with $M(x_1)$ defined in Eqs. (4a)–(4c) such that $M_0 = 0.5$, $M_f = 0$ and $\delta = 1.0°$. It follows that $\alpha_f = M_0 - (\delta/2)(1 - M_f) = 0$. The plunge is linear with $G(x_3) = x_3$. The linear flutter speed $U_L^* = 6.2851$ is determined by solving the aeroelastic system for $M_0 = \delta = \alpha_f = 0$. To obtain an initial guess from the perturbation step, we observe that, for $U^* = U_L^*$, a pair of pure imaginary eigenvalues $\lambda = \pm\omega\mathrm{i} = \pm 0.084\mathrm{i}$ occur in matrix A and the corresponding eigenvectors $\mathbf{u}_1 \pm \mathrm{i}\mathbf{u}_2$ up to a scalar are given by $\mathbf{u}_1 = (0.0208, -0.0022, 0.0404, -0.0063, 0.3404, 0.0865, 0.8868, \ 0.1893)^{\mathrm{T}}$ and $\mathbf{u}_2 = (0.0257, 0.0017, 0.0745, 0.0034, -0.0631, 0.0616, 0, 0.1954)^{\mathrm{T}}$. It follows from Eq. (16) that $p_1 = -4.7471$ and $p_2 = 5.8777$. The traveling time between the two switching point is $T/2 = \pi/\omega = 37.38$.

For the incremental step, we choose the size of the increment ΔU^* to be 0.01. A Hopf-like bifurcation occurs at $U_1^* = U_L^*$ (label 1) where an unstable symmetric LCO is born. The continuation curve of the symmetric LCO is shown in Fig. 6(a). Initially, one eigenvalue of the first derivative $D\Pi$ is outside the unit circle near $+1$. When U^* decreases below $U_2^* = 0.6853U_L^*$ (label 2), the LCO traverses the four main regions. A saddle-node bifurcation occurs at $U_3^* = 0.67892265U_L^*$ (label 3) where an eigenvalue enters the unit circle at $+1$. The enlarged diagram of this region is depicted in Fig. 6(b) which shows a short interval of stable LCO. A symmetry-breaking bifurcation occurs at $U_4^* = 0.67892272U_L^*$ (label 4) and the LCO becomes unstable again. At $U_5^* = 0.678976U_L^*$ (label 5), a harmonic appears in the LCO as its traveling path in $M(x_1)$ branches off from line segment II to line segment V and the trajectory travels in a new linear region R_5. A phase portrait of the unstable LCO with harmonic at $U^* = 0.7U_L^*$ is depicted in Fig. 7. The period, stability and initial switching point X_1 of this LCO with harmonic are given in Table 1. The harmonic disappears at $U_6^* = 0.715U_L^*$ (label 6). As U^* increases beyond the symmetry-breaking bifurcation at $U_7^* = 0.8152U_L^*$ (label 7), the LCO becomes stable again. Its amplitude continues to grow without a bound as U^* tends to U_L^*. A phase portrait of the stable LCO at $U_8^* = 0.85U_L^*$ is shown in Fig. 8 and is compared to the result obtained by using the Runge–Kutta method. They are in good agreement. The dots in Fig. 8 represent the position of the LCO at different time obtained from the PI method. The information of this stable LCO is given in Table 2.

Next, we consider the emanating curve arising from one of the asymmetric LCOs born at U_4^*. On the emanating curve shown in Fig. 9(a), two short intervals of stable LCOs are found near the symmetry-breaking bifurcations. An enlarged diagram near U_4^* is depicted in Fig. 9(b). Period-doubling bifurcation occurs at the other end of the intervals where $U_8^* = 0.679U_L^*$ (label 8) and $U_{11}^* = 0.8127U_L^*$ (label 11). At $U_9^* = 0.6853U_L^*$ (label 9) and $U_{10}^* = 0.7452U_L^*$ (label 10), the LCO intersects tangentially the switching subspace $Z = \alpha_f + \delta = 1$. It will either enter or leave main region III for a small change of U^*. A sudden change of direction in the continuation curve is observed at label 10. This normally occurs when the traveling path of a LCO swops between line segment I or III and line segment V. The asymmetric LCO at label 9 is shown in Fig. 10. It contains a harmonic and its information is given in Table 3. We note that the LCO has an eigenvalue of 4955 which magnitude is very large. In fact, when a LCO corresponds to a sharp turning point on a continuation curve, it always has an eigenvalue with large magnitude.

Emanating curves arising from period-doubling bifurcation at U_8^* and U_{11}^* are shown in Fig. 11(a) (also in Fig. 9(b)) and Fig. 11(b), respectively. There are two short intervals of period-doubling sequences leading to chaos. The one near label 11 was reported in Ref. [10]. Sharp turning points are observed on the period-2 and period-4 emanating branches which are very close to each other. For instance, in Fig. 11(b), these points are at $U_{12}^* = 0.81152U_L^*$ (label 12) and $U_{13}^* = 0.81135U_L^*$ (label 13) for the period-2 and period-4 emanating

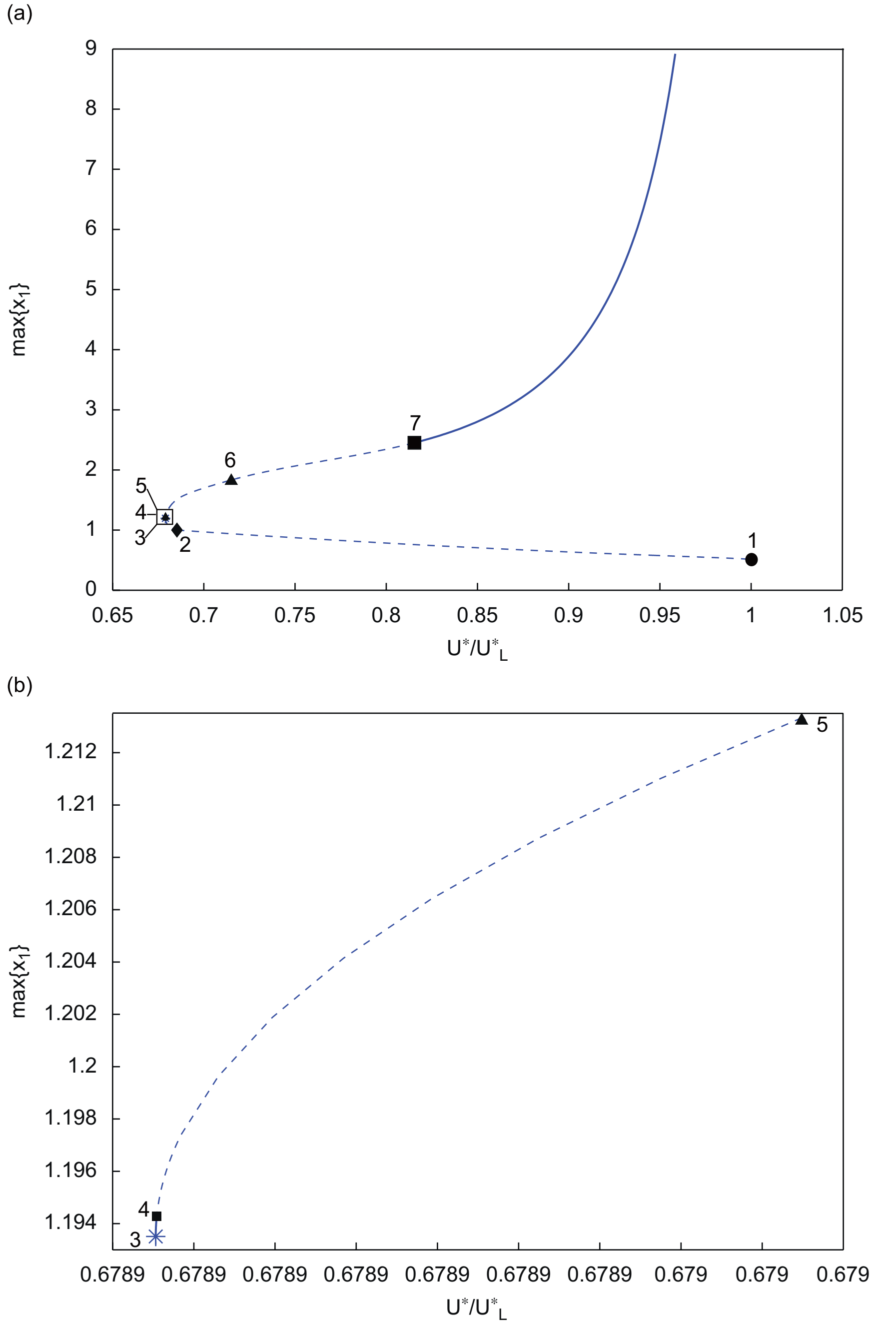

Fig. 6. (a) Continuation curve of symmetric LCO. (b) Enlarged diagram near the saddle-node bifurcation at U_3^*. •, Hopf-like bifurcation; *, saddle-node bifurcation; ■, symmetry-breaking bifurcation.

branches, respectively. It is interesting to note that as $\max(x_1)$ decreases to 1, the asymmetric period-2^n emanating branches arising from period-doubling bifurcation at labels 8 and 11 all join to labels 9 and 10, respectively. This means that when a period-1 LCO enters into main region III from region V at the first time, complicated dynamics suddenly occur which include the coexistence of all period-2^n LCOs and the onset of chaos. Such phenomenon and a sudden change of direction in the continuation curve are not observed in a

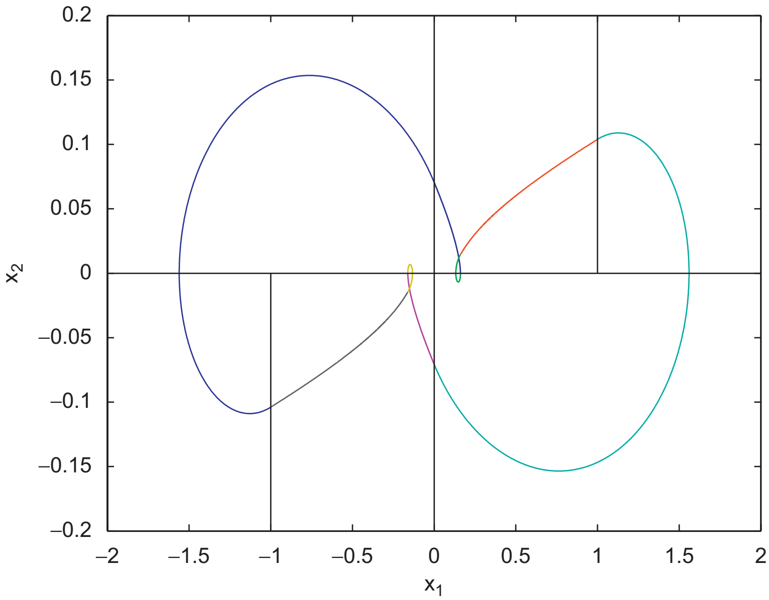

Fig. 7. Unstable symmetric LCO with harmonic at $U^* = 0.7U_L^*$.

Table 1
The period, stability and initial switching point of the LCO with harmonic at $U^* = 0.7U_L^*$

Type of motion: period-1 (symmetric with harmonic)	Period: 105.6
Initial switching point: (−1 − 0.1150 − 10.47 0.1788 − 2.662 − 2.389 − 119.8 − 35.48)	
Eigenvalues of Poincaré map: 2.126, 0.3322, 0.0082, 0.0061, 0.0003, 0, 0	

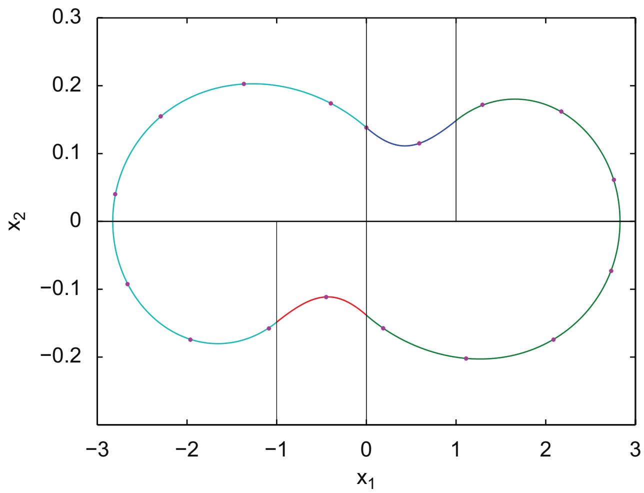

Fig. 8. Stable symmetric LCO at $U^* = 0.85U_L^*$. —, Runge–Kutta method; *, perturbation-incremental method.

two-degree-of-freedom aeroelastic system with freeplay structural nonlinearity [14]. Stable period-2 and period-4 LCOs with harmonic at $U^* = 0.8116U_L^*$ and $U^* = 0.8114U_L^*$ are shown in Fig. 12(a and b), respectively. They are in good agreement with those obtained from the Runge–Kutta method. Their

Table 2
The period, stability and initial switching point of the LCO at $U^* = 0.85U_L^*$

Type of motion: period-1 (symmetric)	Period: 82.78
Initial switching point: $(-1 \quad -0.1469 \quad -6.546 \quad -0.4946 \quad 13.15 \quad -1.914 \quad 24.90 \quad -15.35)$	
Eigenvalues of Poincaré map: $-0.0955+0.1477i,\ -0.0955-0.1477i,\ 0.0400,\ 0.04614,\ 0.0231,\ 0,\ 0$	

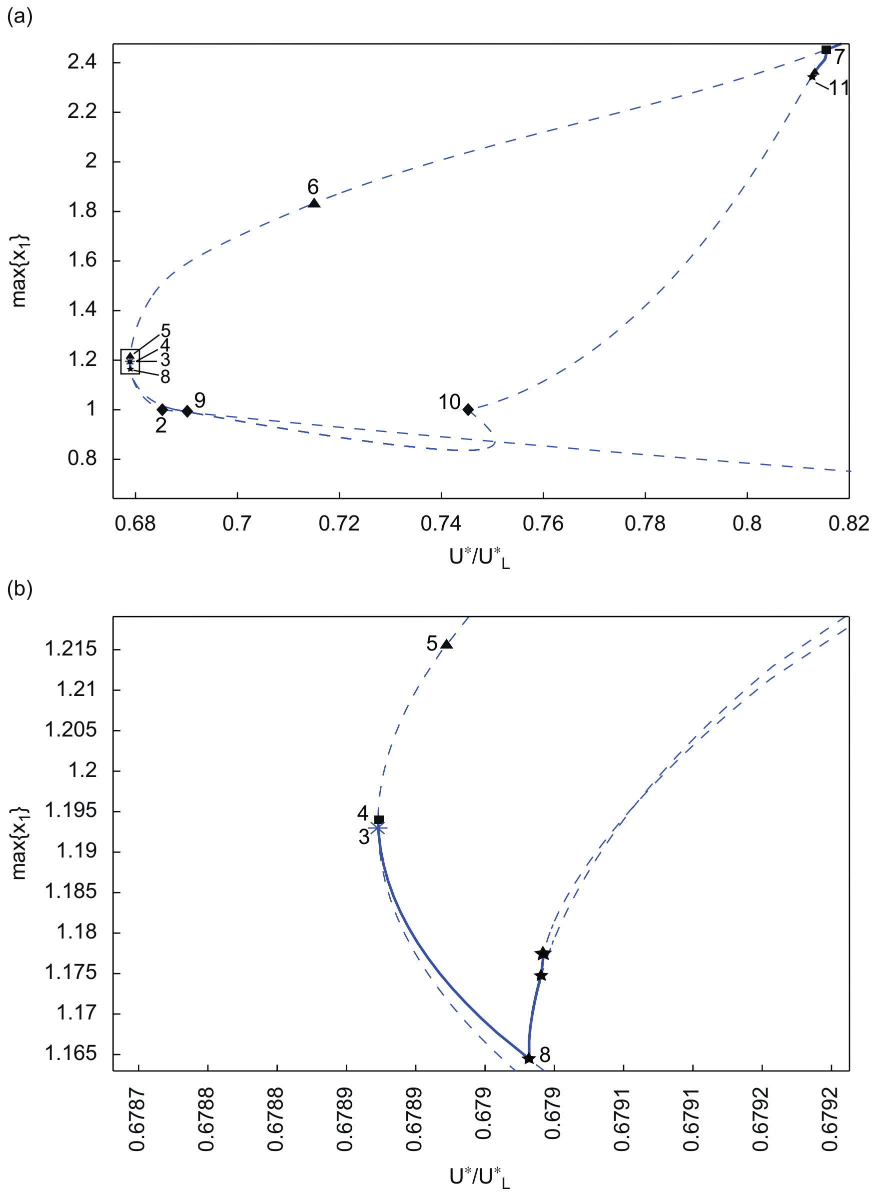

Fig. 9. (a) Continuation curve of one of the asymmetric LCOs. (b) Enlarged diagram near the symmetry-breaking bifurcation at U_4^*. *, saddle-node bifurcation; ■, symmetry-breaking bifurcation; ★, period-doubling bifurcation.

information are given in Tables 4 and 5. A trajectory at $U^* = 0.81\,U_L^*$ obtained from numerical simulation is depicted in Fig. 12(c). This shows a short interval of period-doubling sequence leading to chaos. Emanating branches from both asymmetric LCOs are shown in Fig. 13.

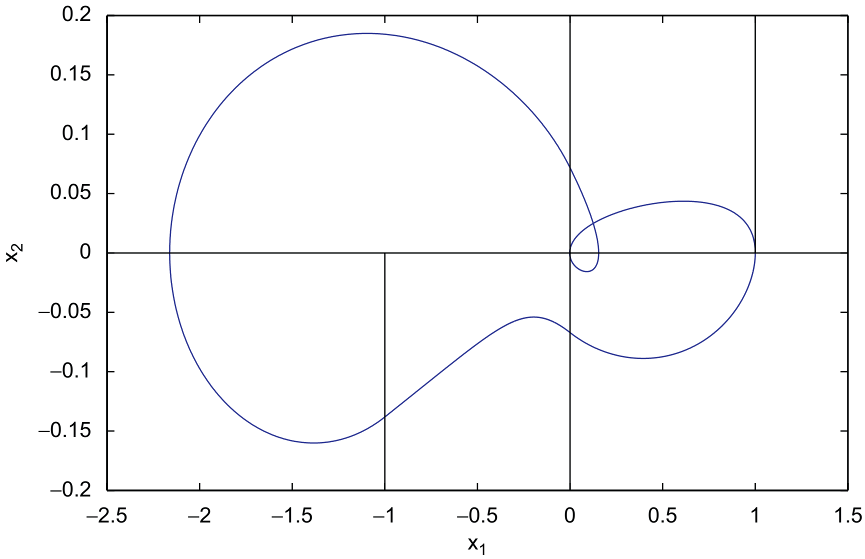

Fig. 10. Unstable asymmetric LCO with harmonic at U_9^*, which intersects tangentially the switching subspace $Z = 1$.

Table 3
The period, stability and initial switching point of the LCO at $U_9^* = 0.6853U_L^*$

Type of motion: period-1 (asymmetric with harmonic)	Period: 112.1
Initial switching point: $(-1 \quad -0.0987 \quad -9.813 \quad 0.2719 \quad -3.460 \quad -2.472 \quad -134.7 \quad -34.41)$	
Eigenvalues of Poincaré map: 4955, 0.4291, 0.0072, 0.0052, 0, 0, 0	

6. Conclusion

A perturbation-incremental (PI) method has been developed to investigate the dynamic response of a self-excited two-degree-of-freedom aeroelastic system with structural nonlinearity represented by a hysteresis stiffness. Since the first derivative of an approximate LCO obtained from the PI method is piecewise continuous which agrees qualitatively with the exact solution, it provides an accurate prediction of the switching points in the switching subspaces where the changes in linear subdomains occur. The present method is also able to compute unstable LCOs and, thus, gives a full picture of the global bifurcation.

A comparison of the dynamic response due to hysteresis and freeplay nonlinearities is discussed below:

(I) *Similarities*
  (i) The stable intervals of period-doubling sequences leading to chaos are very narrow.
  (ii) In the continuation curves, most LCOs are unstable.
(II) *Differences*
  (i) For the hysteresis nonlinearity, a new region is created when the traveling path branches off from line segment II or IV to line segment V. Therefore, the number of regions traversed by a LCO is not fixed. However, for the freeplay nonlinearity, the number of regions is always three.
  (ii) Although the rank of matrix B is 7 for both types of nonlinearities, a trajectory with the hysteresis nonlinearity travels in the eight-dimensional space R_2 or R_4 while that with the freeplay nonlinearity travels in a seven-dimensional subspace of R_2 [14].
  (iii) For the hysteresis nonlinearity, the period-2^n emanating branches are not smooth due to the crossing of a LCO between region R_1 or R_3 and region R_5. Furthermore, all the period-2^n emanating branches join to the sharp turning point where the asymmetric LCO traverses into R_1 or R_3 for the first time

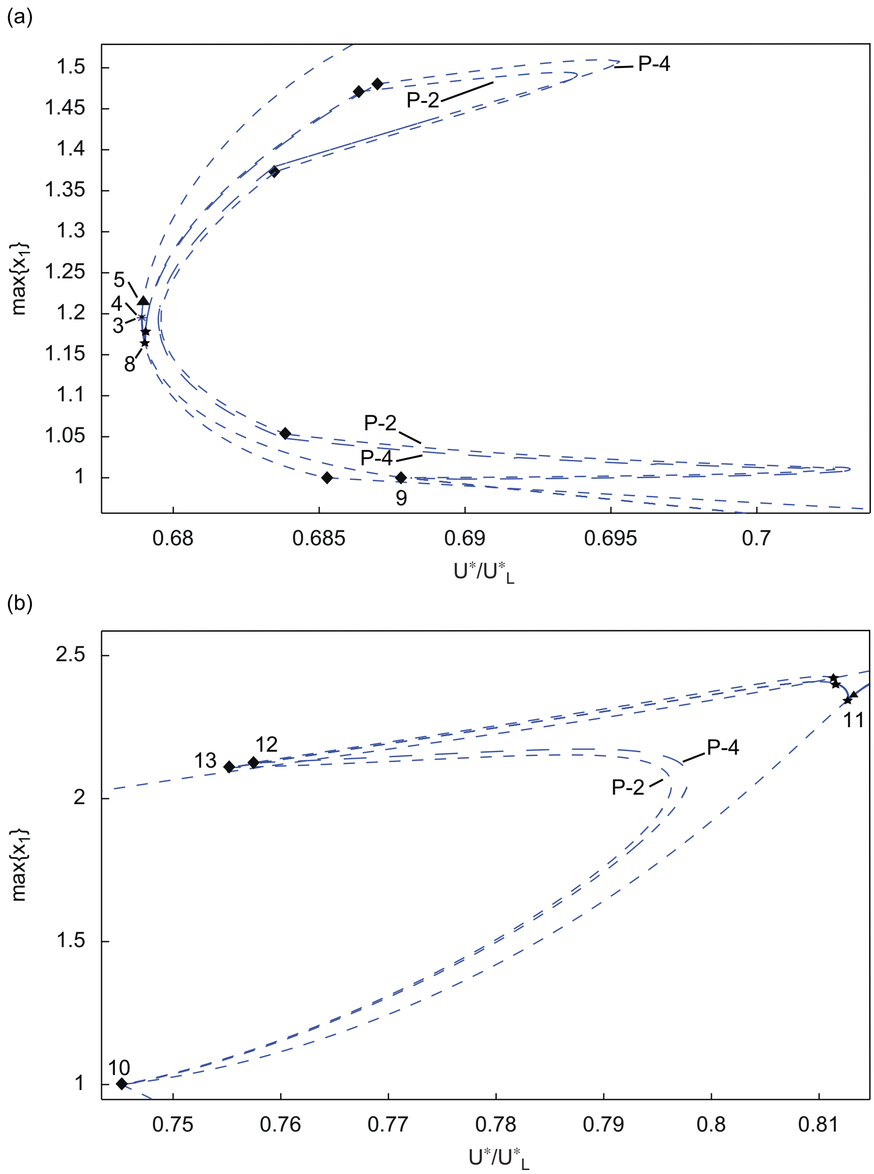

Fig. 11. Period-2 and period-4 emanating branches arising from (a) U_8^* and (b) U_{11}^*.

(see labels 9 and 10 in Fig. 9(a)). However, such dynamic behavior does not occur in an aeroelastic system with freeplay nonlinearity.

(iv) For the hysteresis nonlinearity, Neimark–Sacker bifurcation is not observed. However, such bifurcation is found in the freeplay nonlinearity.

From point (iii) above, when $\max(x_1)(\min(x_1)$, resp.) of a LCO is increased (decreased, resp.) beyond $+1$ (-1, resp.), all period-2^n LCOs come into co-existence. To the best of our knowledge, we are not aware of any piecewise-linear system which exhibits such behavior in the bifurcation of a limit cycle. However, similar phenomenon occurs in a homoclinic bifurcation when the Jacobian of the fixed point of a homoclinic orbit contains double real determining eigenvalue [20,21]. A determining eigenvalue is the one closest to the imaginary axis. Further investigation is needed to see whether the dynamics behind these two phenomena is the same.

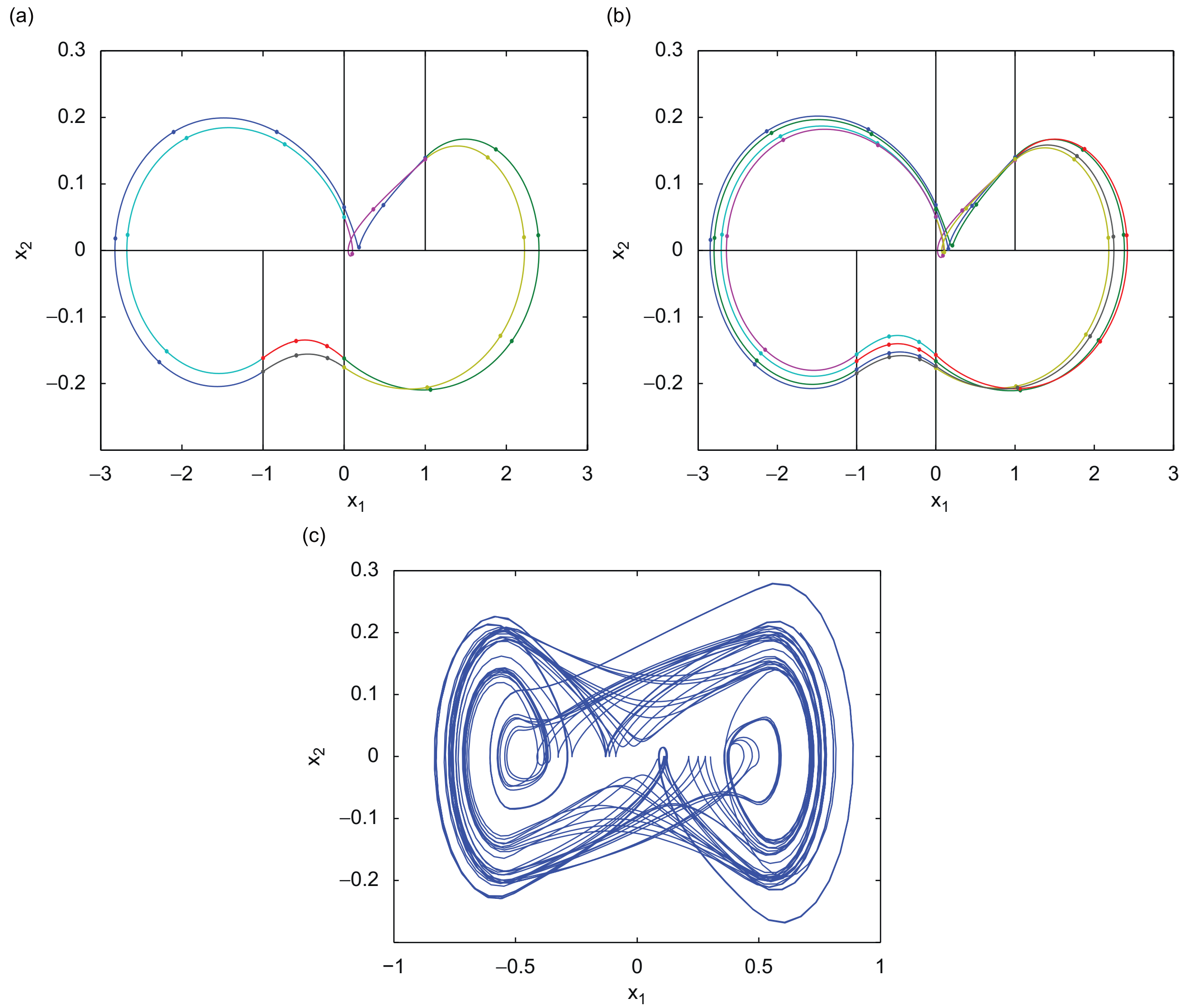

Fig. 12. (a) Stable period-2 LCO with harmonic at $U^* = 0.8116U_L^*$. (b) Stable period-4 LCO with harmonic at $U^* = 0.8114U_L^*$. (c) A trajectory at $U^* = 0.81U_L^*$. —, Runge–Kutta method; *, perturbation-incremental method.

Table 4
The period, stability and initial switching point of the LCO at $U^* = 0.8116U_L^*$

Type of motion: period-2 (asymmetric with harmonic)	Period: 192.3
Initial switching point: $(-1 \quad -0.1820 \quad -6.471 \quad -0.5894 \quad 13.22 \quad -1.458 \quad 65.50 \quad -14.07)$	
Eigenvalues of Poincaré map: $-0.8041, -0.3702, 0.0005, 0.0002, 0, 0, 0$	

Table 5
The period, stability and initial switching point of the LCO at $U^* = 0.8114U_L^*$

Type of motion: period-4 (asymmetric with harmonic)	Period: 384.9
Initial switching point: $(-1 \quad -0.1812 \quad -6.458 \quad -0.5881 \quad 13.22 \quad -1.466 \quad 65.01 \quad -14.04)$	
Eigenvalues of Poincaré map: $-0.8082, -0.1095, 0, 0, 0, 0, 0$	

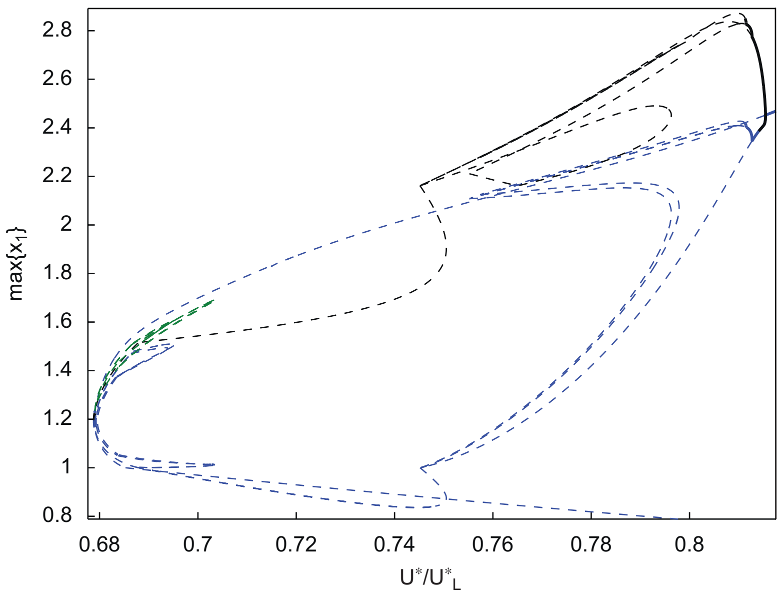

Fig. 13. Emanating branches from both asymmetric LCOs.

Since a traveling path may branch off from line segment II or IV to line segment V, the flow at a point in the phase space may not be unique. Therefore, a trajectory may traverse itself. Although we consider a system of eight ordinary differential equations in this paper, a two-dimensional autonomous piecewise-linear system with hysteresis nonlinearity can also be defined in a similar way. It is well-known that chaos does not occur in a two-dimensional autonomous system because a trajectory never traverses itself. In fact, LCO which traverses itself does exist in a two-dimensional piecewise-linear system with hysteresis nonlinearity [22]. Further study on the possible existence of period-doubling bifurcation and chaos in such a two-dimensional system is undergoing.

Simultaneous coexistence of all period-2^n LCOs are observed in system (3) with hysteresis nonlinearity, but not with freeplay nonlinearity. Likewise, for the celebrated Chua's circuit [23], if the bilinear nonlinearity is replaced by the hysteresis nonlinearity, new bifurcation phenomenon may also occur.

In Refs. [6,10,14] and the present paper, the structural nonlinearity $G(x_3)$ is simply chosen as $G(x_3) = x_3$. In fact, it can be a cubic, freeplay or hysteresis stiffness. In that case, system (3) may contain multiple nonlinearities which are both analytic and non-analytic. The harmonic balance method is usually employed to investigate the dynamic behavior arising from such nonlinearities. For instance, Narayanan and Sekar [24] employed a multi-harmonic balancing technique to capture both stable and unstable solutions of a dynamical system with piecewise linear stiffness and acted on by a flow-induced force with a cubic term. At a switching point, the second derivative of an approximate solution obtained by the harmonic balance method is continuous while that of the exact solution is discontinuous. Therefore, a relatively large number of harmonic terms is required to approximate accurately the exact solution near a switching point. To overcome this problem for system (3) containing multiple nonlinearities, the solution at different nonlinear regions may be approximated by different Fourier series. The continuity of the approximate solution and its derivative at the switching points should be imposed. In this way, the second derivative of an approximate solution is not continuous at a switching point. This is a modified approach to the harmonic balance method. Although the number of unknowns are increased in this formulation, the number of harmonic terms for each Fourier series is less. Further investigation is needed to see whether such formulation is effective.

Acknowledgments

This work was supported by the strategic research grant 7002014 of the City University of Hong Kong. The valuable and constructive comments from the anonymous reviewers are highly appreciated.

Appendix A. Definitions of coefficients

$$a_{21} = j(-d_5c_0 + c_5d_0), \quad a_{41} = j(d_5c_1 - c_5d_1),$$

$$a_{22} = j(-d_3c_0 + c_3d_0), \quad a_{42} = j(d_3c_1 - c_3d_1),$$

$$a_{23} = j(-d_4c_0 + c_4d_0), \quad a_{43} = j(d_4c_1 - c_4d_1),$$

$$a_{24} = j(-d_2c_0 + c_2d_0), \quad a_{44} = j(d_2c_1 - c_2d_1),$$

$$a_{25} = j(-d_6c_0 + c_6d_0), \quad a_{45} = j(d_6c_1 - c_6d_1),$$

$$a_{26} = j(-d_7c_0 + c_7d_0), \quad a_{46} = j(d_7c_1 - c_7d_1),$$

$$a_{27} = j(-d_8c_0 + c_8d_0), \quad a_{47} = j(d_8c_1 - c_8d_1),$$

$$a_{28} = j(-d_9c_0 + c_9d_0), \quad a_{48} = j(d_9c_1 - c_9d_1),$$

where j, c_i $(i = 0, 1, \ldots, 9)$ and d_i $(i = 0, 1, \ldots, 9)$ are defined by

$$j = \frac{1}{c_0d_1 - c_1d_0},$$

$$c_0 = 1 + \frac{1}{\mu}, \quad c_1 = x_\alpha - \frac{a_h}{\mu},$$

$$c_2 = \frac{2}{\mu}(1 - \phi_1 - \phi_2), \quad c_3 = \frac{1}{\mu}[1 + (1 - 2a_h)(1 - \phi_1 - \phi_2)],$$

$$c_4 = \frac{2}{\mu}(\varepsilon_1\phi_1 + \varepsilon_2\phi_2), \quad c_5 = \frac{2}{\mu}\left[1 - \phi_1 - \phi_2 + \left(\frac{1}{2} - a_h\right)(\varepsilon_1\phi_1 + \varepsilon_2\phi_2)\right],$$

$$c_6 = \frac{2}{\mu}\varepsilon_1\phi_1\left[1 - \varepsilon_1\left(\frac{1}{2} - a_h\right)\right], \quad c_7 = \frac{2}{\mu}\varepsilon_2\phi_2\left[1 - \varepsilon_2\left(\frac{1}{2} - a_h\right)\right],$$

$$c_8 = -\frac{2}{\mu}\varepsilon_1^2\phi_1, \quad c_9 = -\frac{2}{\mu}\varepsilon_2^2\phi_2,$$

$$d_0 = \frac{x_\alpha}{r_\alpha^2} - \frac{a_h}{\mu r_\alpha^2}, \quad d_1 = 1 + \frac{1 + 8a_h^2}{8\mu r_\alpha^2},$$

$$d_2 = -\frac{1 + 2a_h}{\mu r_\alpha^2}(1 - \phi_1 - \phi_2), \quad d_3 = \frac{1 - 2a_h}{2\mu r_\alpha^2} - \frac{(1 + 2a_h)(1 - 2a_h)(1 - \phi_1 - \phi_2)}{2\mu r_\alpha^2},$$

$$d_4 = -\frac{1 + 2a_h}{\mu r_\alpha^2}(\varepsilon_1\phi_1 + \varepsilon_2\phi_2), \quad d_5 = -\frac{1 + 2a_h}{\mu r_\alpha^2}(1 - \phi_1 - \phi_2) - \frac{(1 + 2a_h)(1 - 2a_h)(\varepsilon_1\phi_1 - \varepsilon_2\phi_2)}{2\mu r_\alpha^2},$$

$$d_6 = -\frac{1 + 2a_h}{\mu r_\alpha^2}\varepsilon_1\phi_1\left[1 - \varepsilon_1\left(\frac{1}{2} - a_h\right)\right], \quad d_7 = -\frac{1 + 2a_h}{\mu r_\alpha^2}\varepsilon_2\phi_2\left[1 - \varepsilon_2\left(\frac{1}{2} - a_h\right)\right],$$

$$d_8 = \frac{1 + 2a_h}{\mu r_\alpha^2}\varepsilon_1^2\phi_1, \quad d_9 = \frac{1 + 2a_h}{\mu r_\alpha^2}\varepsilon_2^2\phi_2,$$

$$\phi_1 = 0.165, \quad \phi_2 = 0.335, \quad \varepsilon_1 = 0.0455, \quad \varepsilon_2 = 0.3.$$

Appendix B. Definitions of matrices and vectors

$$A_1 = \begin{pmatrix} 0 & 1 & 0 & 0 \\ a_{21} - jc_0\left(\frac{1}{U^*}\right)^2 & a_{22} & a_{23} + jd_0\beta\left(\frac{\bar{\omega}}{U^*}\right)^2 & a_{24} \\ 0 & 0 & 0 & 1 \\ a_{41} + jc_1\left(\frac{1}{U^*}\right)^2 & a_{42} & a_{43} - jd_1\beta\left(\frac{\bar{\omega}}{U^*}\right)^2 & a_{44} \end{pmatrix},$$

$$A_2 = \begin{pmatrix} 0 & 0 & 0 & 0 \\ a_{25} & a_{26} & a_{27} & a_{28} \\ 0 & 0 & 0 & 0 \\ a_{45} & a_{46} & a_{47} & a_{48} \end{pmatrix}, \quad A_3 = \begin{pmatrix} 1 & 0 & 0 & 0 \\ 1 & 0 & 0 & 0 \\ 0 & 0 & 1 & 0 \\ 0 & 0 & 1 & 0 \end{pmatrix}, \quad A_4 = \begin{pmatrix} -\varepsilon_1 & 0 & 0 & 0 \\ 0 & -\varepsilon_2 & 0 & 0 \\ 0 & 0 & -\varepsilon_1 & 0 \\ 0 & 0 & 0 & -\varepsilon_2 \end{pmatrix},$$

$$B_1 = \begin{pmatrix} 0 & 1 & 0 & 0 \\ a_{21} - jc_0 M_f\left(\frac{1}{U^*}\right)^2 & a_{22} & a_{23} + jd_0\beta\left(\frac{\bar{\omega}}{U^*}\right)^2 & a_{24} \\ 0 & 0 & 0 & 1 \\ a_{41} + jc_1 M_f\left(\frac{1}{U^*}\right)^2 & a_{42} & a_{43} - jd_1\beta\left(\frac{\bar{\omega}}{U^*}\right)^2 & a_{44} \end{pmatrix},$$

$$F = \left(0 \quad -jc_0\left(\frac{1}{U^*}\right)^2 \quad 0 \quad jc_1\left(\frac{1}{U^*}\right)^2 \quad 0 \;\; 0 \;\; 0 \;\; 0\right)^{\mathrm{T}}.$$

References

[1] S.F. Shen, An approximate analysis of nonlinear flutter problems, *Journal of the Aeronautical Sciences* 26 (1959) 25–32.

[2] L. Gong, Y.S. Wong, B.H.K. Lee, Dynamics of a coupled system of Duffing's equations, *Dynamics of Continuous, Discrete and Impulsive Systems* 4 (1998) 99–119.

[3] L. Liu, Y.S. Wong, B.H.K. Lee, Application of the centre manifold theory in nonlinear aeroelasticity, *Journal of Sound and Vibration* 234 (2000) 641–659.

[4] S.J. Price, H. Alighanberi, B.H.K. Lee, The aeroelastic response of a two-dimensional airfoil with bilinear and cubic structural nonlinearities, *Journal of Fluids and Structures* 9 (1995) 175–193.

[5] H. Alighanberi, S.J. Price, The post-Hopf bifurcation response of an airfoil in incompressible two-dimensional flow, *Nonlinear Dynamics* 10 (1996) 381–400.

[6] L. Liu, Y.S. Wong, B.H.K. Lee, Non-linear aeroelastic analysis using the point transformation method, Part 1: freeplay model, *Journal of Sound and Vibration* 253 (2002) 447–469.

[7] S.T. Trickey, L.N. Virgin, E.H. Dowell, The stability of limit-cycle oscillations in a nonlinear aeroelastic system, *Proceedings of the Royal Society of London A* 458 (2002) 2203–2226.

[8] E.H. Dowell, R. Clark, D. Cox, H.C. Curtiss Jr., J.W. Edwards, K.C. Hall, D.A. Peters, R. Scanlan, E. Simiu, F. Sisto, T.W. Strganac, *A Modern Course in Aeroelasticity*, fourth ed., Kluwer Academic, Dordrecht, 2004.

[9] B.H.K. Lee, L. Gong, Y.S. Wong, Analysis and computation of nonlinear dynamic response of a two-degree-of-freedom system and its application in aeroelasticity, *Journal of Fluids and Structures* 11 (1997) 225–246.

[10] L. Liu, Y.S. Wong, B.H.K. Lee, Non-linear aeroelastic analysis using the point transformation method, Part 2: hysteresis model, *Journal of Sound and Vibration* 253 (2002) 471–483.

[11] A. Visintin, *Differential Models of Hysteresis*, Springer, Berlin, 1994.

[12] I. Mayergoyz, *Mathematical Models of Hysteresis and Their Applications*, Elsevier, Amsterdam, 2003.

[13] M. Storace, F. Bizzarri, Basic bifurcation analysis of a hysteresis oscillator, *International Journal of Circuit Theory and Applications* 29 (2001) 343–366.

[14] K.W. Chung, C.L. Chan, B.H.K. Lee, Bifurcation analysis of a two-degree-of-freedom aeroelastic system with freeplay structural nonlinearity by a perturbation-incremental method, *Journal of Sound and Vibration* 299 (2007) 520–539.

[15] Y.C. Fung, *An Introduction to the Theory of Aeroelasticity*, Dover, New York, 1993.

[16] R.T. Jones, The unsteady lift of a wing of finite aspect ratio, *NACA Report 681*, 1940.
[17] B.H.K. Lee, S.J. Price, Y.S. Wong, Nonlinear aeroelastic analysis of airfoils: bifurcation and chaos, *Progress in Aerospace Sciences* 35 (1999) 205–334.
[18] A.H. Nayfeh, D.T. Mook, *Nonlinear Oscillations*, Wiley, New York, 1979.
[19] E. Freire, E. Ponce, J. Ros, Limit cycle bifurcation from center in symmetric piecewise-linear systems, *International Journal of Bifurcation and Chaos* 9 (1999) 895–907.
[20] L. Belyakov, The bifurcation set in a system with a homoclinic saddle curve, *Matematicheskie Zametki* 28 (1980) 910–916.
[21] A.R. Champneys, Yu.A. Kuznetsov, Numerical detection and continuation of codimension-two homoclinic bifurcations, *International Journal of Bifurcation and Chaos* 4 (1994) 785–822.
[22] K.W. Chung, Y.B. He, Chaos from a two-dimensional autonomous system with hysteresis nonlinearity, (2008), submitted for publication.
[23] L.O. Chua, M. Komuro, T. Matsumoto, The double scroll family, *IEEE Transactions on Circuits and Systems* CAS-33 (1986) 1072–1118.
[24] S. Narayanan, P. Sekar, Periodic and chaotic responses of an sdf system with piecewise linear stiffness subjected to combined harmonic and flow induced excitations, *Journal of Sound and Vibration* 184 (1995) 281–298.